Ultrafast solvation dynamics explored by femtosecond photon echo spectroscopies

de Boeij, W.P.; Pshenichnikov, M.S; Wiersma, D. A.

Published in:
Annual Review of Physical Chemistry

DOI:
10.1146/annurev.physchem.49.1.99

Annu. Rev. Phys. Chem. 1998. 49:99–123

ULTRAFAST SOLVATION DYNAMICS EXPLORED BY FEMTOSECOND PHOTON ECHO SPECTROSCOPIES

Wim P. de Boeij, Maxim S. Pshenichnikov, and Douwe A. Wiersma
Ultrafast Laser and Spectroscopy Laboratory, Materials Science Centre, University of Groningen, Nijenborgh 4, 9747 AG Groningen, The Netherlands;
e-mail: D.A.Wiersma@chem.rug.nl

KEY WORDS: ultrafast spectroscopy, correlation function

ABSTRACT

Chemical reaction and optical dynamics in the liquid phase are strongly affected by specific solute-solvent interactions. The dynamical part of this coupling leads to energy fluctuations. The associated energy gap dynamics can be probed by using various nonlinear optical spectroscopies. We discuss various forms of photon echo—time-integrated, time-gated, and heterodyne-detected photon echo—as well as Fourier transform spectral interferometry. It is shown that for solutions of the dye molecule DTTCI, a system-bath correlation function can be acquired that provides a quantitative description of all (non)linear spectroscopic experiments. The deduced correlation function is projected onto the multimode Brownian oscillator model, which allows for a physical interpretation of the multiple-time correlation function and a determination of the spectral density relevant to the solvation process. The following applications of photon echo to condensed phase dynamics are discussed: enhanced vibrational mode suppression, Liouville pathways interference, and dynamical Stokes shift. Recent results of echo-peak shift experiments on the hydrated electron are also presented. The review concludes that photon echo should be useful as a novel tool to explore transition state dynamics.

0066-426X/98/1001-0099$08.00

INTRODUCTION

In the last decades, one of the greatest challenges for physical chemistry has been to relate solvent and solvation dynamics to chemical reactivity. Milestones are the work by Kramers (1), who first modeled solvent-assisted barrier crossing, and the work by Marcus & Sutin (2, 3), who laid the foundation for current understanding of electron transfer in solution. Marcus showed that next to the free energy difference between reactant and product, the solvation timescale is also an essential element.

Since these pioneering works, considerable advances have been made, both theoretically (4–21) and in terms of experiments (22–75) testing these theories. For instance, on the theoretical side, the models to describe electron transfer have become more refined by including low- and high-frequency molecular vibrations explicitly into the calculations (22). Also, the description of solvent dynamics has become more realistic by allowing solvent fluctuations to occur on multiple timescales (18–21) instead of one, as in the original Marcus theory. Progress was also made in a description of solvation dynamics on a microscopic scale by molecular dynamics simulations (6–14) and the connection of the solvation to fluorescence Stokes shift dynamics. Successful attempts were also made to describe solvation dynamics in terms of instantaneous normal modes (15–17). Despite the appeal of this approach, its usefulness remains to be tested and some problems, for instance the interpretation of the imaginary frequencies, remain to be adressed.

An important link between theory and condensed phase dynamics was made by the development of the multimode Brownian oscillator (MBO) model (18, 19). This heuristic model allows for a simple interpretation of system-bath (SB) dynamics in terms of overdamped and underdamped oscillators. These oscillators can be viewed as solvent (or solute) degrees of freedom that are strongly coupled to the electronic states of interest. An equally important asset of the MBO model is that it provides a direct connection between experimental observables in linear and nonlinear optical spectroscopy and the rate of an electron-transfer reaction (20, 21).

Although from a theoretical perspective it has been clear that measuring the solvation dynamics is important to further progress in our comprehension of electron transfer, experimentally the timescales for these liquid state dynamics, ranging from tens of femtoseconds to milliseconds, could not be covered before femtosecond lasers were developed (76–79).

Although optical spectra are determined by the full range of the solute-solvent dynamics, the retrieval of these dynamics from the spectra alone is impossible. It turns out that nonlinear optical spectroscopic techniques provide the key to map out the dynamics of the solute-solvent coupling underlying the

optical lineshape (23–75). In case of solutions, pump-probe (45–47), transient hole burning (48, 49), resonance Raman scattering [50, see also the review by Myers (51) in this volume], and photon echo (23–44) have been extensively used. Below we discuss the concept of photon echo in greater detail. For pure solvents, Rayleigh/Raman scattering (52–55), Raman echo (56–58), and optical Kerr effect (59–69) have been explored.

Femtosecond photon echo is well suited to probe solvation dynamics, because it creates a time window through which this dynamical process can be monitored (80). In the MBO model the decay of the photon echo is connected to solvation dynamics by the correlation function $M(t)$:

$$M(t) = \frac{\langle \delta\omega(0)\ \delta\omega(t)\rangle}{\langle \delta\omega^2\rangle}, \qquad 1.$$

where $\delta\omega(t)$ is the time-dependent optical transition frequency of the solvated molecule and $\langle \cdots \rangle$ indicates a statistical average over the ensemble. The solute-solvent coupling is thus projected into the SB correlation function $M(t)$.

In this review we show that $M(t)$ can be obtained by the use of different photon echo techniques. Although several of these echo techniques are not simple to implement in the laboratory, there is one notable exception: the so-called echo-peak shift (EPS) method. This method, first applied by De Silvestri et al (73, 74), recently made its comeback after it was shown (75) that the EPS function tracks the SB correlation function remarkably well, except at very early times. Because photon echo probes the loss of coherence as well as the flow of population in a system, the EPS method will rapidly gain ground as a tool to probe condensed phase dynamics.

EXPERIMENTAL

For an experiment to be a success, a number of conditions must be met. Below we review briefly some prerequisites for a proper photon echo experiment.

Excitation Pulse Energy

To stay within the limits of the $\chi^{(3)}$ perturbative approximation, the excitation pulses should rotate the Bloch vector over only a few degrees (81). Typical dye molecules used have a dipole moment of about 1 D, implying that for a 10-fs pulse only 25 nJ is needed to generate a $\pi/2$-area pulse. This result shows that, in principle, a conventional continuous wave, mode-locked Ti:sapphire laser could be used for femtosecond photon echo experiments. However, for time-gated echo and higher-order spectroscopies (32, 33, 63–69), a continuous wave mode-locked laser is not powerful enough.

Single-Shot Regime

To avoid accumulation of long-lived photoproducts, which can severely distort the signals, photon echo experiments should be done in the single-shot regime, where the system has completely relaxed. Another approach uses a new sample in every measurement, as can be achieved by use of a jet or by high-speed spinning of the sample. At typical sample speeds of 0.1–10 m/s, repetition rates of 5–500 kHz are allowed. Clearly, a conventional continuous wave, femtosecond Ti:sapphire, operating at 80 MHz, cannot be used, and either pulse picking or cavity dumping (yielding higher pulse energies as well) is necessary.

Cavity-Dumped Ti:Sapphire Laser

A simple and convenient way to generate higher-pulse intensities is to incorporate a cavity dumper into the resonator (82, 83). In this manner, 13-fs, 60-nJ pulses can be generated at variable repetition rates. This laser can also easily be tuned (84) in the range of 760–860 nm, though at the expense of the pulse duration (∼25 fs). The short pulse duration, high peak power, variable repetition rate, and excellent stability of the cavity-dumped Ti:sapphire laser have been crucial to the success of the experiments described in this review.

THEORETICAL APPROACH

The interaction between an optically active chromophore and the solvent is described by a specific set of generalized solvation coordinates (Figure 1*a*). In the case of a linear coupling, these coordinates are represented by displaced harmonic oscillators. A direct consequence of this approach is that the optical dynamics of the system and in particular the energy gap fluctuations [characterized by the energy gap correlation function $M(t)$] are isomorphic with the nuclear dynamics of the generalized solvation coordinates. Knowledge of the dynamics of these solvation coordinates thus suffices to characterize the complete optical dynamics of the system. For a phenomenological description of the molecular motions in liquids, the MBO model will be employed (18, 19). In this model, the solvation coordinates are coupled to a set of harmonic bath modes. Here we assume that the spectral distribution of these bath modes is uniform (Ohmic disspiation). With this particular choice of the bath, analytical expressions for the solvation coordinates can be derived. These enable the evaluation of the correlation function $M(t)$ or, equivalently, the spectral density $C(\omega)$. From either of these functions, the complex lineshape function $g(t)$ can be derived (Figure 1*b*), from which the steady-state absorption and emission spectra can be calculated. From a cumulant expansion, the nonlinear response functions $R(t_1, t_2, t_3)$ are obtained as a linear combination of line shape functions, taken at times $t_1, t_2, t_1 + t_2$, etc. Finally, the induced

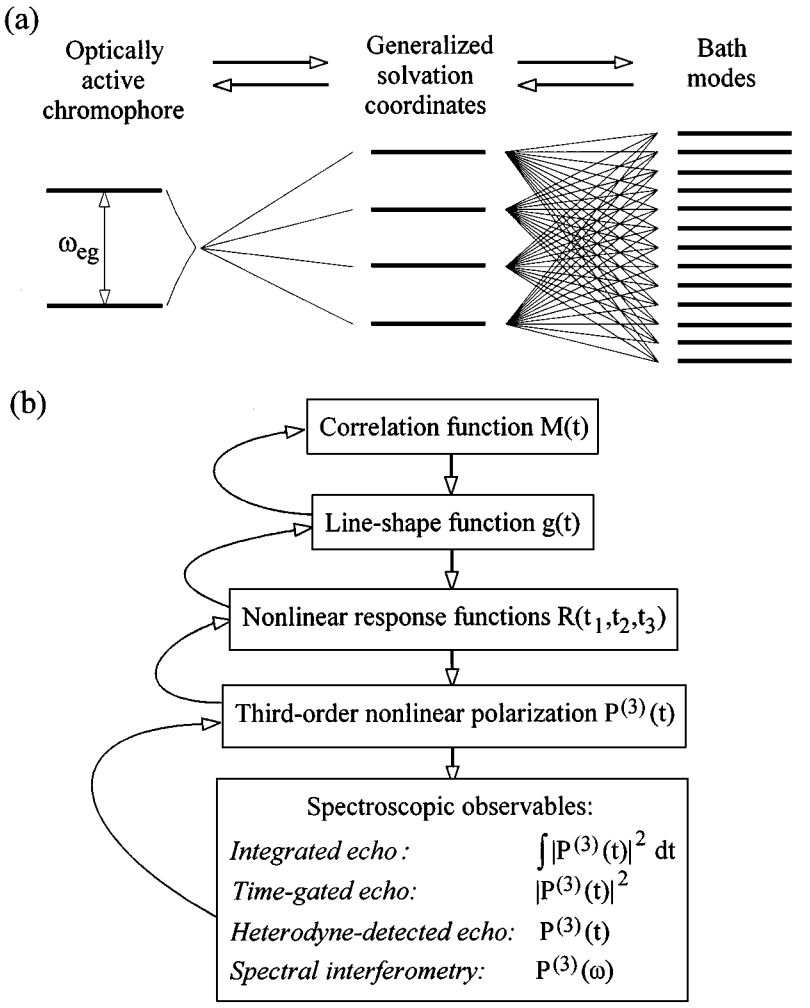

Figure 1 (*a*) Schematics of the interaction between the optical chromophore and the solvent bath in the framework of the Brownian oscillator model. The generalized solvation coordinates present those solvent modes that couple to the solute. ω_{eg} denotes the frequency of electronic transition. (*b*) The sequence of transformations from the system-bath correlation function to spectroscopic observables.

third-order nonlinear polarization $P^{(3)}(t)$ is expressed as a convolution of the response function with the excitation fields. Depending on the experimental conditions, one observes specific projections of the polarization (Figure 1*b*), which can be probed experimentally. In this paper, we discuss time-integrated, time-gated, and heterodyne-detected photon echo and spectral interferometry (Figure 1*b*). Once the induced polarization is fully characterized, the SB correlation function can be retrieved.

PHOTON ECHO SPECTROSCOPIES

Photon Echo: a Holographic Probe

Photon echo (81) is an optical response from a hologram written in frequency space. This hologram or frequency grating (85) is actually a fringe pattern of the form $\cos(\Delta - k_{12} \cdot r + \phi_{12})$, created in the sample's optical spectrum by the effect of two excitation pulses at a delay time τ. In the cos function, Δ is the difference between the carrier frequency of the light field and the frequency of the absorber, whereas k_{12} and ϕ_{12} are the wave vector and phase difference, respectively, between the first two excitation pulses. The upper inset in Figure 2 depicts the frequency grating that is created after its formation [around $M(t) = 1$] in the ground state. In the excited state, a similar hologram

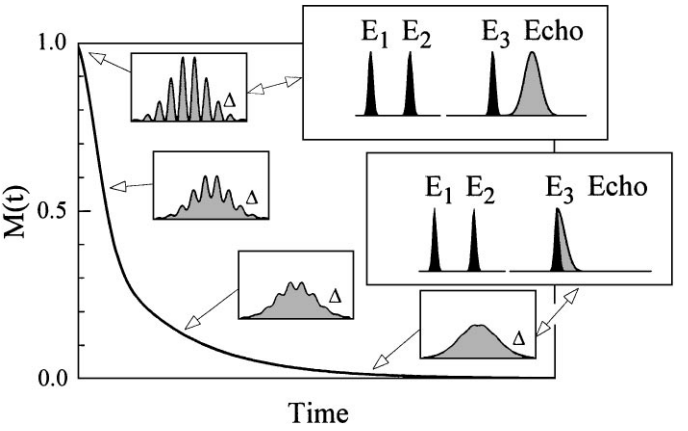

Figure 2 System-bath correlation function and associated decays of the frequency grating formed in the ground state. Δ denotes the frequency detuning from the optical transition. The excitation pulse sequence E_1-E_3 as well as the emitted signals are depicted for $M(t) = 1$ (inhomogeneous broadening) and $M(t) = 0$ (homogeneous broadening). Note that in the former case, the signal is delayed with respect to the last excitation pulse (photon echo), whereas in the latter case, the signal maximum coincides with the last excitation pulse (free induction decay).

is formed but phase shifted by 180 degrees. These holograms fade in time by relaxation processes, which reduce the amplitude and contrast of the fringes (Figure 2). When the holograms are probed after a certain delay (waiting time), each hologram is read out, thereby generating a coherent response, called photon echo. The intensity of the echo field is related to the sum of the grating amplitudes in the ground and excited state, which decay through fluctuations of the transition frequencies, described by the correlation function $M(t)$. The decay of the echo signal with time is therefore directly related to the solute-solvent dynamics.

To take advantage of the phase-match condition, photon echo experiments are often performed with the excitation pulses crossed at a small angle. In this way, the echo is launched into a direction different from any of the excitation pulses. In the simplest case, the signal is recorded using a slow detector, for instance a photodiode. More advanced detection schemes employ time-gating (37, 38) or heterodyning (34, 70–72). It is also possible to retrieve the echo using spectral interferometry (86). The various techniques are addressed below.

Time-Integrated Detection: the Echo-peak Shift Measurement

The time-integrated stimulated photon echo (SPE) signal can be expressed as follows:

$$S_{\mathrm{INT}}(t_{23}, t_{12}) = \int_0^\infty \left| P^{(3)}_{\mathrm{SPE}}(t, t_{23}, t_{12}) \right|^2 dt. \qquad 2.$$

Here, P_{SPE} denotes the third-order polarization, whereas t_{12} and t_{13} are the delays between the first two pulses and the first and third pulses, respectively. It has been shown that SPE intensity measurements as a function of the delays t_{12} and t_{23} provide no direct information on the SB dynamics, unless there is a strict separation of timescales [Bloch limit (28, 87)].

Evidently, for solutions, a more direct probe of the correlation function is desired. More than a decade ago, it was shown that the EPS is an excellent probe of optical dynamics (73, 74). A direct link between the EPS and a dynamical model, however, was not made. Recently, however, the EPS method revived, after it had been shown that there is a direct connection between the EPS and the amplitude of the SB correlation function at the selected waiting time (41, 75). In an EPS experiment (Figure 3*a*), the integrated photon echo intensity is measured for a fixed delay t_{23} while scanning t_{12} (Figure 3*b*). The shift of the echo maximum with respect to zero delay along the t_{12} axis constitutes the observable, the so-called EPS. It was demonstrated that a plot of the EPS as a function of waiting time t_{23} tracks the SB correlation function, except at the

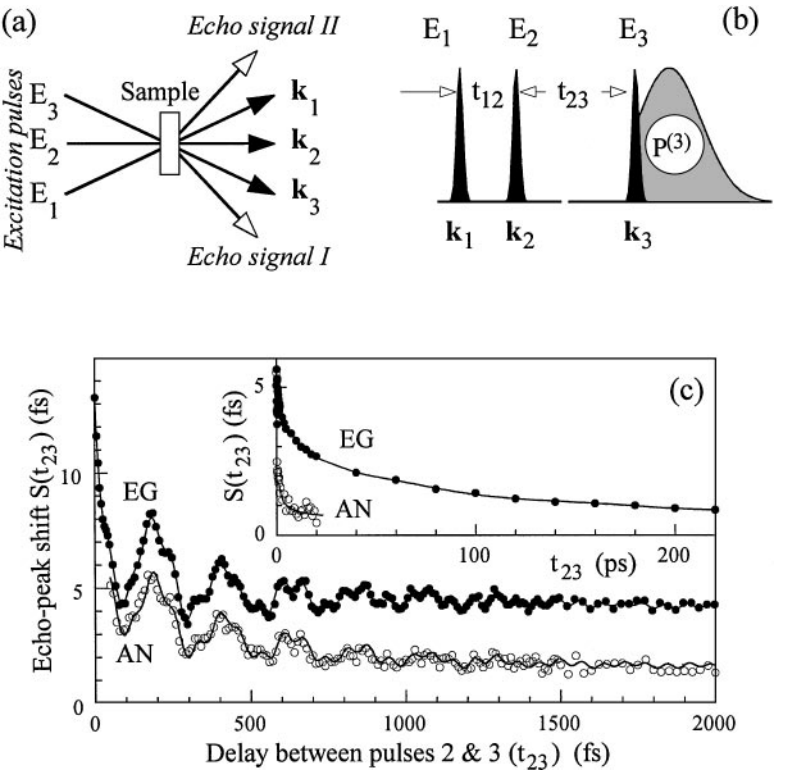

Figure 3 Integrated stimulated photon echo. (*a*) Schematics of the experiment, and (*b*) the time sequence of the applied pulses. Two echo signals (I and II) are detected in phase-matched directions. Definitions of the delays and wavevectors and an artist's impression of the emitted nonlinear signal are given. (*c*) The results of an echo-peak shift experiment performed on the dye molecule DTTCI dissolved in ethylene glycol (*solid circles*) and acetonitrile (*open circles*). (*solid lines*) Fits with the multimode Brownian oscillator model. (*inset*) The long timescale dynamics.

earliest times (42, 75):

$$M(t_{23}) = \frac{\Delta\sqrt{\pi}\,S_{\mathrm{EPS}}(t_{23})}{1 + 2\Delta^2 S^2_{\mathrm{EPS}}(t_{23})}, \qquad 3.$$

where $S_{\mathrm{EPS}}(t_{23})$ is the measured EPS at delay t_{23} and Δ is the coupling strength parameter.

Experimentally, a precise measurement of the EPS is made as follows: Two echo signals in conjugate phase-matched directions $k_3 + k_2 - k_1$ and $k_3 + k_1 - k_2$ are recorded simultaneously (Figure 3*a*). The EPS is then calculated as

half the distance between the two corresponding maxima of the profiles fitted with a smooth function (e.g. polynomial or Gaussian). Using this procedure, the experimental precision can be as high as 0.2 fs. An example is shown in Figure 3*c*, based on a few hundred measurements.

The quantum beats in the EPS function are due to wave packet dynamics in ground and excited states (42). Because these dynamics are solvent independent, these beats must reflect intrachromophore vibrational dynamics. In contrast, the solute-solvent dynamics vary greatly between solvents. For instance, in ethylene glycol (EG) the EPS decays on a timescale of 50–200 ps, whereas in acetonitrile this timescale is approximately 3 ps. The long timescale dynamics in EG is, most likely, caused by diffusive solvent motion.

Although the EPS method can be used to determine the correlation function in various systems [for instance, dye solutions (34, 41, 42), dye-doped polymers (88), and biological systems (89)], it only yields a first-order estimate of the correlation function. Further improvement of this function is obtained by numerical calculations, which include the actual pulse shape (42). Furthermore, the correlation function that emerges from the EPS measurement should be substantiated by other experiments and simulations thereof.

Time-Gated Photon Echo Spectroscopy

As noted above, there are fundamental reasons why the EPS method fails to yield the initial part of the correlation function (34, 42). A more advanced—yet more elaborate—detection scheme employs time-gating, where the echo signal is mixed with a gate pulse in a nonlinear optical crystal (Figure 4*a*) (37, 38, 42). For a gate pulse that is short compared with the temporal width of the echo, the signal at the sum frequency maps out the echo as a function of time t_g (Figure 4*b*):

$$S_{\text{gated}}(t_g, t_{23}, t_{12}) \propto \left| P^{(3)}_{\text{SPE}}(t_g, t_{23}, t_{12}) \right|^2 \times |E_g(t_g)|^2. \qquad 4.$$

One important observable concerns the maximum of the echo intensity profile ($t_{\max}$) (42) as a function of the pulse delays t_{12} and t_{13}. In a typical time-gated echo experiment, the position of the echo maximum $t_{\max}$ is plotted as a function of t_{12} (Figure 4*c*). The apparent break point in the curve at $t_{12} \approx 30$ fs signifies the presence of, at least, two distinctly different timescales in the correlation function. This break point reflects the average correlation time τ_c of the fast part of the correlation function:

$$\tau_c = \int_0^\infty M_{\text{fast}}(t)\, dt. \qquad 5.$$

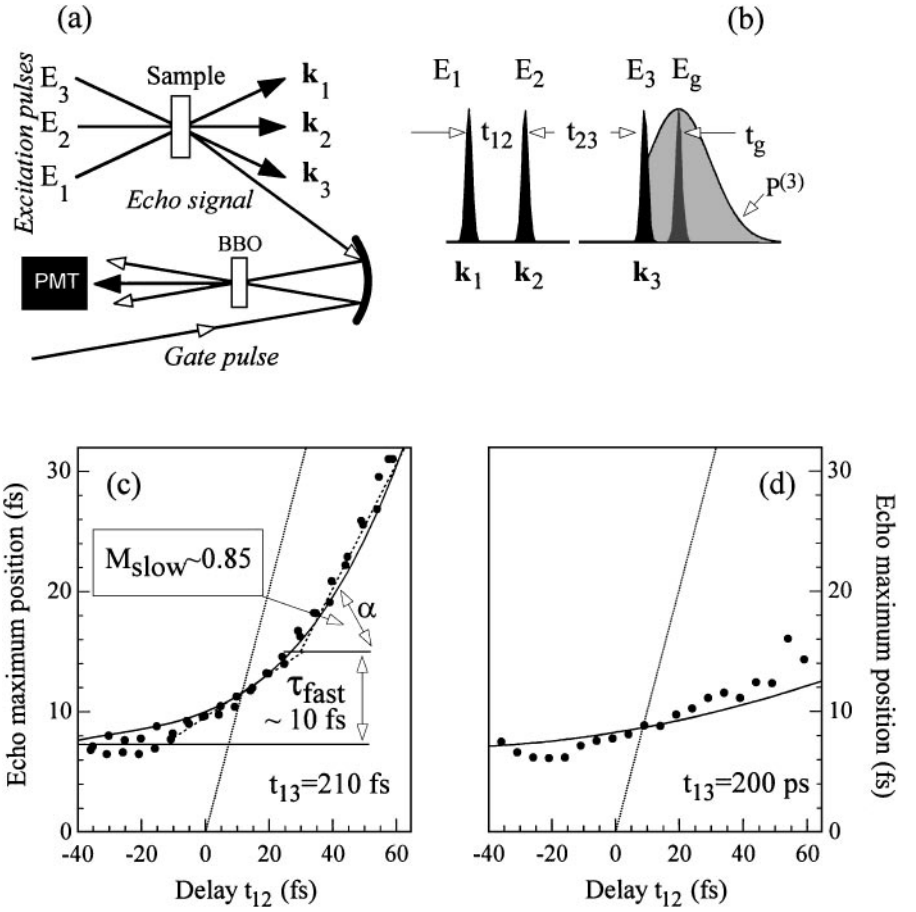

Figure 4 Time-gated stimulated photon echo. (*a*) Schematics of the experiment, (*b*) the time sequence of the applied pulses, and (*c*, *d*) results of a time-gated experiment performed on the dye molecule DTTCI dissolved in ethylene glycol at waiting times $t_{13} = 210$ fs and 200 ps (respectively). The echo signal emitted in the phase-matched direction is mixed with the gate pulse in a 25-μm thick β-barium borate (BBO) crystal. (*dotted lines*) Echo maxima expected for an overwhelming inhomogeneous broadening. The ~7-fs offset is caused by the effect of finite pulse duration. (*circles*) Experimental points; (*solid lines*) fits to the multimode Brownian oscillator model.

The slow part of the echo-maximum curve equals the slope at long times t_{12} (Figure 4*c*):

$$\left(\frac{\partial t_{\max}}{\partial t_{12}}\right)_{t_{12}\to\infty} = \operatorname{arctg}(\alpha) = M_{\text{slow}}(t_{23}). \qquad 6.$$

From the fits, given as solid lines in Figure 4*c*, we obtain $\tau_c \sim 10$ fs and $M_{\text{slow}}(t_{13} = 210 \text{ fs}) \sim 0.85$. A 10-fs correlation time is consistent with earlier time-gated, two-pulse echo experiments (37).

With increasing waiting time t_{13}, the slope of the echo-maximum curves decreases, eventually changing the echo-maximum curve from slightly upward-bending to an almost straight line (Figure 4*d*). At this point, the loss of phase memory has transformed the echo into a free-induction-decay-like signal (see also the insets in Figure 2).

Comparing the EPS with time-gated echo, it is clear that the latter provides more detailed information on the correlation function. On the other hand, the EPS method is a much simpler technique.

Heterodyne-Detected Photon Echo

EPS and time-gated echo are both homodyne-type experiments, which implies that the information on the phase of the induced polarization is lost. Such data, however, is crucial if one wants to get facts on the time dependence of the mean energy, as reflected in the dynamical Stokes shift. To get access to the phase of the induced polarization, a heterodyne-detected photon echo (HSPE) experiment (34, 70–72, 84, 90) needs to be performed.

In a HSPE experiment, the fourth field, $E_4(t)$, serves as local oscillator, $E_{\text{LO}}(t)$, in heterodyne detection (Figure 5*a*) of the induced polarization (Figure 5*b*):

$$S_{\text{HSPE}}(t_{34}, t_{23}, t_{12}) \propto \text{Im}\left[P^{(3)}(t_{34}, t_{23}, t_{12}) \times E^*_{\text{LO}}(t_{34})\right]. \qquad 7.$$

In contrast to time-gated echo, which probes the modulus square of the polarization (Equation 4), the heterodyne-detected signal is directly proportional to the induced polarization. Furthermore, by controlling the optical phase between the signal and local oscillator, the in-phase (real) and in-quadrature (imaginary) components of the nonlinear polarization can be probed, from which the amplitude and phase of the polarization and the nonlinear response functions can be determined.

Experimentally, phase control is achieved by using an actively stabilized Mach-Zehnder interferometer (91–93). To properly define a spatially independent optical phase between the pulses, the wavevectors of the first and the second excitation pulses need to be equal: $k_1 = k_2$ (Figure 5*b*). Two phase differences

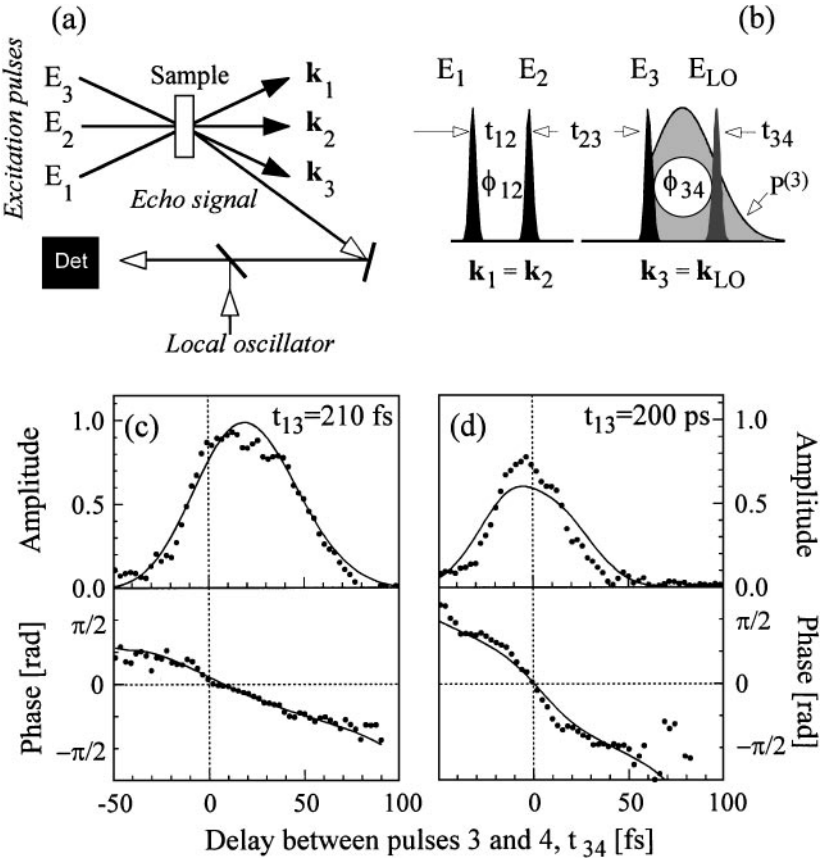

Figure 5 Heterodyne-detected stimulated photon echo. (*a*) Schematics of the experiment, (*b*) the time sequence of the applied pulses, and (*c, d*) the amplitude and phase of the echo signal from the dye molecule DTTCI in ethylene glycol for $t_{12} = 40$ fs at waiting times $t_{13} = 210$ fs and 200 ps (respectively). The echo signal emitted in the phase-matched direction is mixed with the local oscillator pulse on the quadratic detector (Det). The phase differences between pulse pairs E_1-E_2 and E_3-E_{LO} are denoted as ϕ_{12} and ϕ_{34}, respectively. (*circles*) Experimental points; (*solid lines*) fits with the multimode Brownian oscillator model.

thus play a role: the relative phase ϕ_{12} between the first pulse pair (E_1-E_2) and the phase difference ϕ_{34} for the second pulse pair (E_3-E_4).

It has been shown (72, 84) that for impulsive excitation, a measurement of phase-orthogonal HSPE signals (i.e. with $\phi_{12}, \phi_{34} = 0, \pi/2$) permits a full reconstruction of the echo amplitude

$$S_{\text{echo}} \propto \sqrt{[S_{\text{HSPE}}(0,0) + S_{\text{HSPE}}(\pi/2,\pi/2)]^2 + [S_{\text{HSPE}}(\pi/2,0) - S_{\text{HSPE}}(0,\pi/2)]^2}, \quad 8.$$

and phase

$$\Phi_{\text{echo}} = \arctan\left\{\frac{S_{\text{HSPE}}(\pi/2,0) - S_{\text{HSPE}}(0,\pi/2)}{S_{\text{HSPE}}(0,0) + S_{\text{HSPE}}(\pi/2,\pi/2)}\right\}, \quad 9.$$

where the arguments stand for the phases ϕ_{12} and ϕ_{34}, respectively. Note that the derivative of the echo phase (Equation 9) with respect to t_{34} gives the instantaneous frequency of the echo signal.

A full set of phase-orthogonal HSPE signals (71, 72, 84) was measured, from which the echo fields were reconstructed (Figure 5*c*, *d*), using Equations 8 and 9. For a waiting time of 210 fs, the echo amplitude peaks near $t_{34} \sim 20$ fs, consistent with time-gated echo experiments (Figure 4*c*). For a waiting time of 200 ps, all phase memory is lost—the system is homogeneously broadened at this point—and the amplitude of the induced polarization peaks near $t_{34} = 0$ (Figure 5*d*).

Inspection of Figure 5*c* and *d* shows that the phase varies linearly with the delay t_{34}. This indicates that the instantaneous frequency is constant at the timescale over which t_{34} is scanned. If t_{13} increases, the phase-vs-t_{34} curve becomes steeper, indicating a red shift of the emission. In fact, this instantaneous frequency-shift tracks the dynamical Stokes shift, usually measured by fluorescence up-conversion (vide infra). Note that both the Bloch (87) and the Kubo model (94) cannot handle such frequency shifts.

Spectral Interferometry

Spectral interferometry (86) can be viewed as the frequency-domain analog of HSPE. Rather than monitoring the interference between the signal and the local oscillator in the time domain (HSPE), spectral interferometry explores their interference in the frequency domain. From the spectral interferogram one can readily deduce the spectral amplitude and phase of the signal field, provided the reference pulse has been completely characterized (95–99). The main advantage of spectral interferometry compared with HSPE is that the full

spectrum can be taken in a single shot, using an optical multichannel analyser, without having to measure the echo signal as a function of delay time t_{34}.

Spectral interferometry can easily be done by a slight adjustment of the HSPE setup (Figure 6*a*). However, there are two important differences. The first is that three instead of four pulses are needed. The second distinction is that the signal is dispersed through a polychromator prior to being detected by an optical multichannel analyzer. Note that the third excitation pulse acts also as the

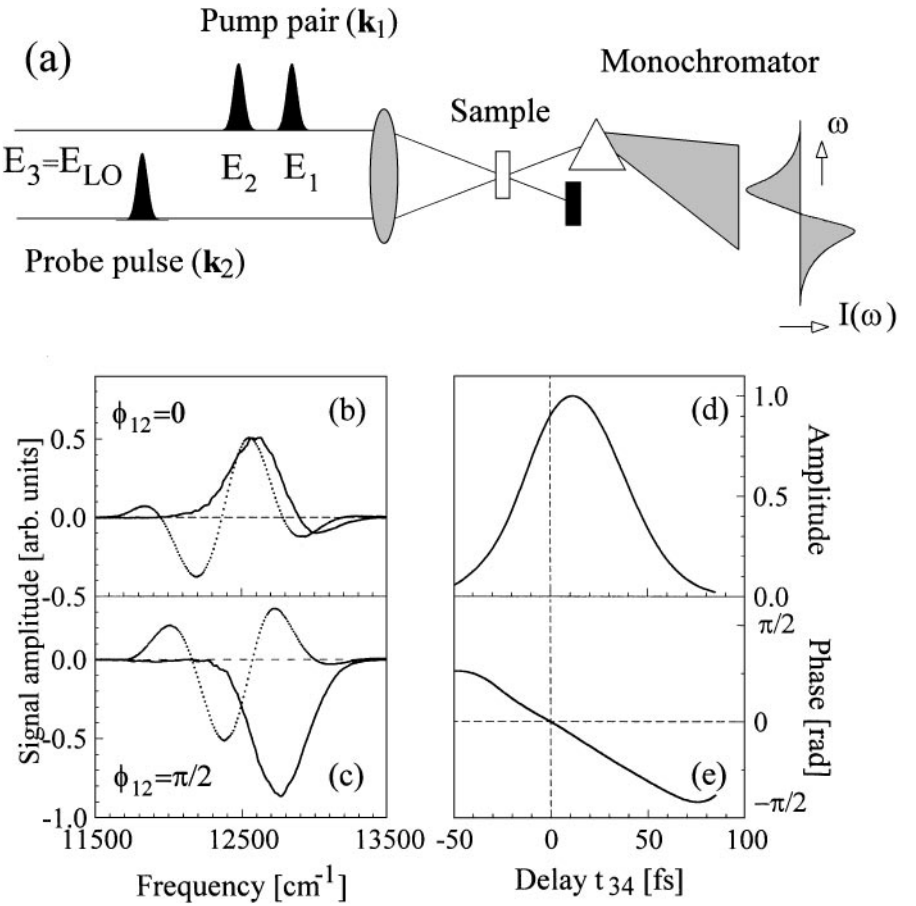

Figure 6 Spectral interferometry. (*a*) Schematics of the experiment, (*b*, *c*) spectral interferograms (*solid lines*) at $t_{12} = 40$ fs for $\phi_{12} = 0$ and $\pi/2$ (respectively), and (*d*, *e*) calculated amplitude and phase (respectively) of the echo signal from the dye molecule DTTCI dissolved in ethylene glycol. The waiting time is set to $t_{13} = 210$ fs. (*dotted lines*) The measured interferogram ($\mathrm{Re}[E_1(\Omega)E_2^*(\Omega)]$) of the excitation pulse pair.

reference pulse, implying that all information on the induced polarization with respect to any of the excitation pulses is conserved. The recorded spectral interferogram is proportional to the imaginary part of the induced nonlinear polarization:

$$S(\Omega, t_{12}, t_{13}, \phi_{12}) \propto \mathrm{Im}\left[P^{(3)}(\Omega, t_{12}, t_{13}, \phi_{12})\right]. \quad 10.$$

From Fourier-transformation of Equation 10, while taking into account that the polarization obeys causality [i.e. $P^{(3)}(t, t_{12}, t_{13}, \phi_{12}) \equiv 0$ for $t < 0$], the following relation can be derived (100):

$$P^{(3)}(t, t_{12}, t_{13}, \phi_{12}) \propto \int_{-\infty}^{\infty} d\,\Omega\, \exp(i\Omega t) S(\Omega, t_{12}, t_{13}, \phi_{12}). \quad 11.$$

In general, Equation 11 yields a complex value for $P^{(3)}(t, t_{12}, t_{13}, \phi_{12})$. Performing two phase-orthogonal measurements, the transient echo amplitude can be derived (84):

$$S_{\mathrm{echo}} \propto P^{(3)}(t, t_{12}, t_{13}, \phi_{12} = 0) - i\,P^{(3)}(t, t_{12}, t_{13}, \phi_{12} = \pi/2), \quad 12.$$

from which the temporal amplitude and phase of the echo signal can be calculated.

Figure 6*b* and *c* shows the spectrally resolved signals measured for $\phi_{12} = 0$ and $\phi_{12} = \pi/2$. Note that the interferograms are different from the excitation spectra. This is a clear signature of dephasing occurring during the time intervals t_{12} and t_{13} (86).

Calculated according to Equation 12, the amplitude and the phase of the echo signal (Figure 6*d, e*) are in close agreement with those obtained previously (Figure 5*c*). However, because the nonlinear polarization $P^{(3)}(t)$ has a non-zero amplitude for $t < 0$ in the case of finite pulse duration, the assumption made in the derivation of Equation 11 is not strictly fulfilled. This causes the maximum of the calculated echo profile to be slightly shifted toward shorter delays. Nonetheless, the spectral interferometry method presents an easy and simple alternative to the more accurate but tedious time-domain HSPE technique (42).

DISCUSSION

The System-Bath Correlation Function

To relate the experimental data to the energy-gap correlation function, the MBO model was employed (19). The EPS and time-gated echo-maxima functions (Figure 3) were used as a first-order approximation to the slow and fast part of the correlation function, respectively. From here on, iterative numerical calculations were performed to achieve the best fit to all data (Figures 3–5)

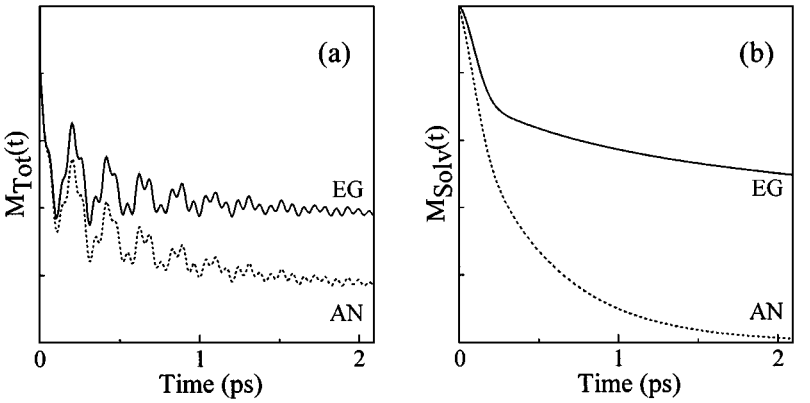

Figure 7 (*a*) Total system-bath correlation function and (*b*) the extracted solvation correlation function for the dye molecule DTTCI dissolved in ethylene glycol (*solid line*) and acetonitrile (*dashed line*).

(42). The resulting SB correlation functions of DTTCI in EG and acetonitrile (Figure 7*a*) reflect the intrachromophore dynamics as well as the chromophore-solvent dynamics. The initial fast decay (on a 10-fs timescale) is attributed to energy redistribution among intrachromophore modes. The fastest solvation process takes place on a 100-fs timescale, whereas at slightly longer times, the decay of the prominent low-frequency intrachromophore mode occurs. On a 1-ps timescale, diffusive solvent motion occurs. The decay times of prominent high-frequency intramolecular modes proceeds on the same timescale. On longer timescales (∼10–100 ps, not shown), still slower diffusional processes occur as well as reorientational relaxation. Finally, the optical cycle is completed by population relaxation on a 1-ns timescale.

So far, the dye's optical transition has been described in terms of an electronic two-level system interacting with a bath comprised of both intra- and intermolecular degrees of freedom (Figure 1*a*). Elimination of the intrachromophore dynamics from the total SB correlation function leaves the bare solvation correlation function (Figure 7*b*). The ultrafast part of the depicted correlation functions (∼200 fs for EG and ∼150 fs for acetonitrile) is, most likely, linked to inertial solvation dynamics. The picosecond timescale part of the correlation function (up to 200 ps for EG) is attributed to a diffusive type of solvent motions.

Spectral Density of Solute-Solvent Interaction

Once the SB correlation function has been obtained, one can readily calculate the corresponding spectral density via a Fourier-transformation (Figure 8) (19).

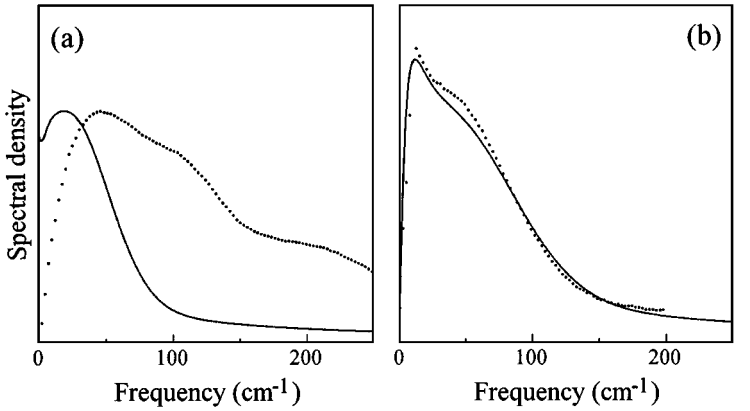

Figure 8 Solvent spectral density for (*a*) acetonitrile and (*b*) ethylene glycol. (*solid lines*) Spectral densities obtained by Fourier-transformation of the solvation correlation function (Figure 7*b*); (*dotted lines*) experimental spectral densities obtained from the optical Kerr effect (acetonitrile from Reference 59 and ethylene glycol from Reference 60). The data are arbitrarily normalized.

It has been suggested (35, 36, 38, 101) that solvation dynamics is induced by the same solvent motions that are probed in the optical Kerr effect (59–62). Figure 8*b* shows that for acetonitrile, the agreement between these spectral densities is remarkable, showing that in this solvent the solvent modes with the largest anisotropic polarizabilities are the ones that relax the optical dipole (35, 36, 101).

For EG, a hydrogen-bonded solvent, the optical Kerr effect spectral density and the one derived from the SB correlation function overlap only at low frequencies, where the spectrum is mainly determined by collision-induced effects. Higher-frequency solvent motions seem to have little impact on the solvation process in EG (59, 61, 102). A similar discrepancy occurs for methanol (42), pointing at our lack of understanding of solvation processes on a microscopic level.

SELECTED RESULTS

Heterodyne-Detected Photon Echo as Alternative to Fluorescence Upconversion

In the framework of the MBO model, the instantaneous frequency of the HSPE signal is directly proportional to $M(t)$ (72, 84):

$$\omega_{\text{inst}}(t_{13}) = \partial\Phi(t_{13}, t_{34})/\partial t_{34} = \lambda[M(t_{13}) - 1]. \qquad 13.$$

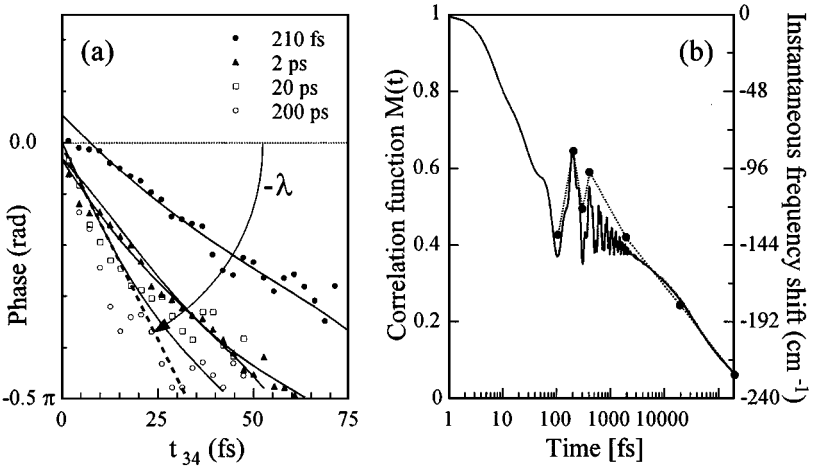

Figure 9 (*a*) Time-dependent phase of the nonlinear third-order polarization as measured with the heterodyne-detected stimulated photon echo technique. (*b*) Functional behavior of the correlation function $M(t)$ as used in the calculations. The points in panel *b* mark the position of the instantaneous frequency shift at the different delays t_{13}, as obtained from a linear fit to the data presented in panel *a*. (*solid lines*) Fits to the multimode Brownian oscillator model; (*dashed line*) the maximum possible inclination determined by the steady-state Stokes shift; (*arrow*) for long times t_{13}, the frequency shift approaches $-\lambda$.

Figure 9*a* presents the time-dependent phase of the HSPE signal for different waiting times t_{13}. A nearly linear time dependence of the phase on the delay t_{34} is observed, implying a constant instantaneous frequency of the emitted polarization. Figure 9*a* shows that with increasing delay t_{13}, the phase-vs-t_{34} curves exhibit a greater negative slope. For long times t_{13}, the frequency shift approaches $-\lambda$, which is in fact the average of the Stokes shift in the ground state (0) and the excited state (-2λ).

The deduced instantaneous frequency shift reflects directly the system correlation function (Figure 9*b*). HSPE is therefore an alternative—although not easy to implement—to conventional fluorescence up-conversion methods (22, 103–108) in measurement of the correlation function. It is especially useful in systems that exhibit a moderate Stokes shift.

Enhanced Vibrational Mode Suppression

Molecular electronic transitions are often strongly coupled to molecular vibrations. In order to capture the genuine solute-solvent dynamics, intramolecular wave packet dynamics either have to be accounted for in the analysis of the data

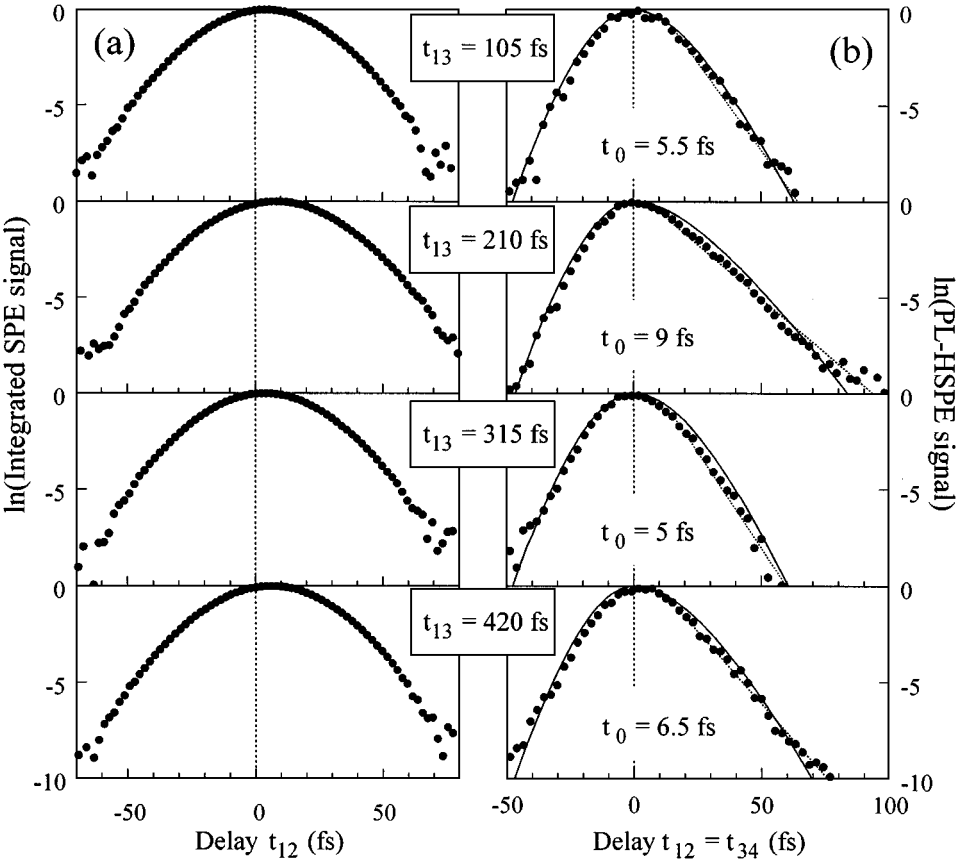

Figure 10 Mode-suppression in (*a*) time-integrated and (*b*) time-gated stimulated photon echo. Diagonal time-gated signals are obtained from heterodyne detected photon echo signals. (*dotted lines*) Fits to the time-gated echo signals with the function t_{12}/t_0; (*circles*) experimental points; (*solid lines*) fits to the multimode Brownian oscillator model.

or suppressed in the experiment. Suppression of a single vibrational mode can be accomplished if the third excitation pulse is delayed with respect to the first one by the inverse vibrational frequency (109, 110). The system behaves then as if it were a pure two-level system. However, this method works well only for solids where inhomogeneous broadening is overwhelming. In solution, where homogeneous and inhomogeneous broadening are of the same order, the echo decays and profiles are virtually independent of whether the third pulse is in or out of phase with the rephasing wave packet (Figure 10*a*).

In this case, mode suppression can be accomplished by diagonal time-gating ($t = t_{12}$) of the SPE (111). Diagonal time-gated SPE leads to enhanced mode suppression for systems that exhibit multiple timescale dynamics (Figure 10*b*). For $t_{13} = 210$ fs, where maximal mode suppression is expected, the slope of the signal is almost linear, signifying exponential decay of the echo, with a time constant of about 9 fs. For longer waiting times, the time-gated echo decays faster because of the vibrational dephasing. Another factor contributing to a faster echo decay is the transition from an inhomogeneous to a more homogeneous system.

Liouville-Pathway Interference and Coherent Control

The existence of multiple excitation pathways invites the exploration of Liouville-pathway interference effects in HSPE (49). Interference occurs between the conventional and the virtual echo polarization, which in HSPE are emitted in the same direction (112–114). The setting of the relative phases of the excitation pulses determines whether the interference between the conventional and virtual echoes is constructive or destructive. If $\phi_{12} = 0$, the echo fields interfere constructively, resulting in an enhanced signal (Figure 11*a*). In contrast, if $\phi_{12} = \pi/2$, a phase shift of π occurs between the conventional and virtual echo fields. The resulting destructive interference leads to suppression of the signal at long delays t_{13} (Figure 11*b*). At the longest delays, the real and virtual echoes have merged, and the signal vanishes by destructive interference of equally intense but oppositely phased fields. Therefore, active control of the

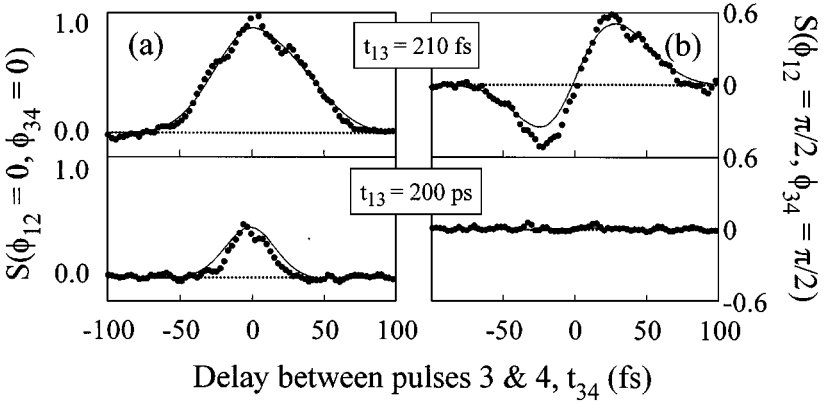

Figure 11 Heterodyne detected stimulated photon echo signals for the dye molecule DTTCI in ethylene glycol, measured with phase settings (*a*) $\phi_{12} = 0$, $\phi_{34} = 0$ and (*b*) $\phi_{12} = \pi/2$, $\phi_{34} = \pi/2$ for waiting times $t_{13} = 210$ fs and 200 ps. The delay t_{12} is set at 55 fs. (*circles*) Experimental points; (*solid lines*) fits to the multimode Brownian oscillator model.

relative phases allows for switching between constructive and destructive interference. This phase-locked excitation scheme is of special interest to coherent control experiments in chemistry, where Liouville-space pathway interference is thought to be an important option (115–117).

Ultrafast Hydrated-Electron Dynamics

The aqueous electron (118) is one of the simplest physical systems to study, therefore grasp of its dynamics is extremely important. It is unique in the sense that it provides the opportunity to confront results of state-of-the-art nonlinear optical experiments (119–129) with quantum molecular dynamics simulations (130–139). The hydrated electron is also important from a chemical point of view, as water is one of the most important solvents in chemistry. Because water has a large dipole moment and exhibits strong hydrogen bonding, its dynamics are often strongly coupled to the reaction path, especially when electronic charges are being shifted.

Figure 12 presents results of EPS measurements on the hydrated electron, along with the deduced correlation function. The figure shows that excellent agreement exists between the calculated EPS based on the assumed correlation function. These ultrafast photon echo experiments also clearly resolve the wave packet dynamics in the coherent response of the hydrated electron. This wave packet feature is assigned to librational motions of water molecules, forming the cage in which the electron is trapped. Interestingly enough, this phenomenon has not been predicted by quantum-molecular dynamics simulations. Photon echo experiments on the hydrated with sub-5-fs optical pulses (140, 141) are

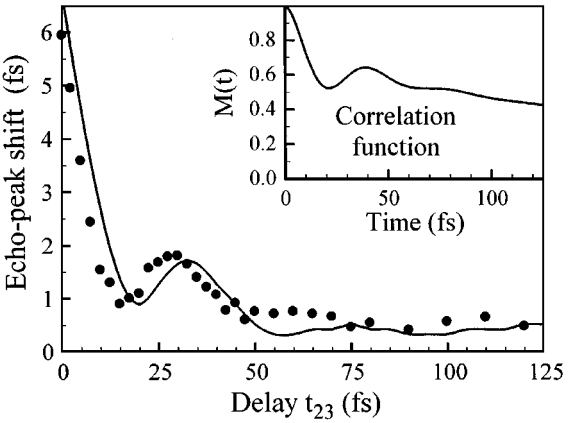

Figure 12 Experimental (*solid circles*) and simulated (*lines*) echo-peak shift function for the hydrated electron. (*inset*) The correlation function used in simulations.

currently in progress. Such experiments should also reflect the intra-p-state dynamics not captured by the present experiments.

CONCLUSIONS AND PROSPECTS

Using a variety of photon echo experiments, we have determined the SB correlation function of a dye molecule in solution. The physics of the correlation function was analyzed in terms of under- and overdamped Brownian oscillators, representing intramolecular vibrations and solvent motions, respectively. The spectral density of the solvent motions, which dominate the solvation response, agrees well with the spectral density obtained from optical Kerr effect measurements in the case of acetonitrile, but in the case of EG and other hydrogen-bonded solvents only the low-frequency parts overlap. This indicates that polarizability changes are not the only factor determining the effectiveness of the solute-solvent coupling.

The fact that only a few Brownian oscillators are needed to simulate the complex optical dynamics of a dye molecule in solution validates the use of the MBO model for liquid state dynamics. The next step is to project this parametrization onto a more microscopic model.

The next challenge is to employ photon echo as a probe of reactive dynamics, for instance electron- and proton-transfer reactions, which are key processes in nature. In electron- and proton-transfer reactions, the solvent (or protein) responds to a change of electronic or protonic state by solvent shell (or protein nuclear) reorganization. An ultrafast study of reactive systems, aiming at a grasp of the interplay between reactive and solvent dynamics, seems promising. Photon echo is particularly suited to address these issues because it senses both electronic and vibrational coherences. In addition to single-color photon echo, two-color photon echo, which relies on correlations of the solvation response, should be explored.

ACKNOWLEDGMENTS

We are grateful to R Szipöcs and K Ferenz for specially designed optics and to MF Emde and A Kummrow for their participation in some of the experiments. The investigations were supported by the Netherlands Foundation for Chemical Research (Stichting Scheikundig Onderzoek Nederland, SON) and Physical Research (Stichting voor Fundamenteel Onderzoek der Materie, FOM), with financial aid from the Netherlands Organization for the Advancement of Science (Nederlandse Organisatie voor Wetenschappelijk Onderzoek, NWO).

Literature Cited

1. Kramers HA. 1940. *Physica* 7:284–304
2. Marcus RA, Sutin N. 1985. *Biochem. Biophys. Acta* 811:275–322
3. Sumi H, Marcus RA. 1986. *J. Chem. Phys.* 84:4894–914
4. Grote RF, Hynes JT. 1980. *J. Chem. Phys.* 73:2715–32
5. Grote RF, Hynes JT. 1981. *J. Chem. Phys.* 74:4465–75
6. van der Zwan G, Hynes JT. 1985. *J. Phys. Chem.* 89:4181–88
7. Hänggi P, Talkner P, Borkovec M. 1990. *Rev. Mod. Phys.* 62:250–341
8. Carter EA, Hynes JT. 1991. *J. Chem. Phys.* 94:5961–79
9. Neria E, Nitzan A. 1992. *J. Chem. Phys.* 96:5433–40
10. Perera L, Berkowitz ML. 1992. *J. Chem. Phys.* 97:5253–54
11. Maroncelli M. 1993. *J. Mol. Liq.* 57:1–37
12. Kumar PV, Maroncelli M. 1995. *J. Chem. Phys.* 103:3038–60
13. Roy S, Bagchi B. 1993. *J. Chem. Phys.* 99:9938–43
14. Bagchi B. 1994. *J. Chem. Phys.* 100: 6658–64
15. Stratt RM, Cho M-H. 1994. *J. Chem. Phys.* 100:6700–8
16. Ladanyi BM, Stratt RM. 1995. *J. Phys. Chem.* 99:2502–11
17. Stratt RM. 1995. *Acc. Chem. Res.* 28:201–8
18. Tanimura Y, Mukamel S. 1993. *Phys. Rev. E* 47:118–36
19. Mukamel S. 1995. *Principles of Nonlinear Optical Spectroscopy*. New York: Oxford Univ. Press
20. Yan YJ, Spargaglione M, Mukamel S. 1988. *J. Phys. Chem.* 92:4842–53
21. Mukamel S, Yan YJ. 1989. *Acc. Chem. Res.* 22:301–8
22. Barbara PF, Walker GC, Smith TP. 1992. *Science* 256:975–81
23. Becker PC, Fragnito HL, Bigot J-Y, Cruz CHB, Fork RL, Shank CV. 1989. *Phys. Rev. Lett.* 63:505–7
24. Pollard WT, Fragnito HL, Bigot J-Y, Shank CV, Mathies RA. 1990. *Chem. Phys. Lett.* 168:239–45
25. Bigot J-Y, Portella MT, Schoenlein RW, Bardeen CJ, Migus A, Shank CV. 1991. *Phys. Rev. Lett.* 66:1138–41
26. Nibbering ETJ, Wiersma DA, Duppen K. 1991. *Phys. Rev. Lett.* 66:2464–67
27. Joo T, Albrecht AC. 1993. *Chem. Phys.* 176:233–47
28. Nibbering ETJ, Wiersma DA, Duppen K. 1994. *Chem. Phys.* 183:167–85
29. de Boeij WP, Pshenichnikov MS, Duppen K, Wiersma DA. 1994. *Chem. Phys. Lett.* 224:243–52
30. Bardeen CJ, Shank CV. 1994. *Chem. Phys. Lett.* 226:310–16
31. Rosenthal SJ, Schwartz BJ, Rossky PJ. 1994. *Chem. Phys. Lett.* 229:443–48
32. Cho M-H, Fleming GR. 1994. *J. Chem. Phys.* 98:3478–85
33. Joo T, Jia Y-W, Fleming GR. 1995. *J. Phys. Chem.* 102:4063–68
34. de Boeij WP, Pshenichnikov MS, Wiersma DA. 1995. *Chem. Phys. Lett.* 238: 1–8
35. Vöhringer P, Arnett DC, Westervelt RA, Feldstein MJ, Scherer NF. 1995. *J. Chem. Phys.* 102:4027–36
36. Yang T-S, Vöhringer P, Arnett DC, Scherer NF. 1995. *J. Chem. Phys.* 103:8346–59
37. Pshenichnikov MS, Duppen K, Wiersma DA. 1995. *Phys. Rev. Lett.* 74:674–77
38. Vöhringer P, Arnett DC, Yang T-S, Scherer NF. 1995. *Chem. Phys. Lett.* 237: 387–98
39. Joo T-H, Jia Y-W, Yu J-Y, Lang MJ, Fleming GR. 1996. *J. Chem. Phys.* 104:6089–108
40. Cho M-H, Yu J-Y, Joo T-H, Nagasawa Y, Passino SA, Fleming GR. 1996. *J. Phys. Chem.* 100:11944–53
41. Fleming GR, Cho M-H. 1996. *Annu. Rev. Phys. Chem.* 47:109–34
42. de Boeij WP, Pshenichnikov MS, Wiersma DA. 1996. *J. Phys. Chem.* 100:11806–23
43. Passino SA, Nagasawa Y, Fleming GR. 1997. *J. Chem. Phys.* 107:6094–108
44. Passino SA, Nagasawa Y, Joo T, Fleming GR. 1997. *J. Phys. Chem.* 101:725–31
45. Fragnito HL, Bigot J-Y, Becker PC, Shank CV. 1989. *Chem. Phys. Lett.* 160:101–4
46. Pollard WT, Lee S-Y, Mathies RA. 1990. *J. Chem. Phys.* 92:4012–29
47. Bardeen CJ, Wang Q, Shank CV. 1995. *Phys. Rev. Lett.* 75:3410–13
48. Ma J, Vanden Bout D, Berg M. 1995. *J. Chem. Phys.* 103:9146–60
49. Bingemann D, Ernsting NP. 1995. *J. Chem. Phys.* 102:2691–700
50. Myers AB. 1997. *Acc. Chem. Res.* 30: 519–27
51. Myers AB. 1998. *Annu. Rev. Phys. Chem.* 49:267–95
52. Myers AB, Li BL, Ci X-P. 1988. *J. Chem. Phys.* 89:1876–86
53. Myers AB, Li BL. 1988. *J. Chem. Phys.* 92:3310–22

54. Goldberg SY, Bart E, Meltsin A, Fainberg BD, Huppert D. 1994. *Chem. Phys.* 183: 217–34
55. Fainberg BD. 1993. *Phys. Rev. A* 48:849–50
56. Vanden Bout D, Muller LJ, Berg M. 1991. *Phys. Rev. Lett.* 67:3700–3
57. Muller LJ, Vanden Bout D, Berg M. 1993. *J. Chem. Phys.* 99:810–19
58. Inaba R, Tominaga K, Tasumi M, Nelson KA, Yoshihara K. 1993. *Chem. Phys. Lett.* 211:183–88
59. McMorrow D, Lotshaw WT. 1991. *J. Phys. Chem.* 95:10395–406
60. Chang YJ, Castner EW Jr. 1993. *J. Chem. Phys.* 99:113–25
61. Deuel H, Cong P, Simon JD. 1994. *J. Phys. Chem.* 98:12600–8
62. Vöhringer P, Scherer NF. 1995. *J. Phys. Chem.* 99:2684–95
63. Steffen T, Duppen K. 1996. *Phys. Rev. Lett.* 76:1224–27
64. Steffen T, Fourkas JT, Duppen K. 1996. *J. Chem. Phys.* 105:7364–82
65. Steffen T, Duppen K. 1997. *J. Chem. Phys.* 106:3854–64
66. Tominaga K, Yoshihara K. 1995. *Phys. Rev. Lett.* 74:3061–64
67. Tominaga K, Yoshihara K. 1996. *J. Chem. Phys.* 104:1159–62
68. Tominaga K, Yoshihara K. 1996. *J. Chem. Phys.* 104:4419–26
69. Tokmakoff A, Lang MJ, Larsen DS, Fleming GR, Chernyak V, Mukamel S. 1997. *Phys. Rev. Lett.* 79:2702–5
70. de Boeij WP, Pshenichnikov MS, Wiersma DA. 1995. *Chem. Phys. Lett.* 247: 264–70
71. Pshenichnikov MS, de Boeij WP, Wiersma DA. 1995. *Phys. Rev. Lett.* 76: 4701–4
72. de Boeij WP, Pshenichnikov MS, Wiersma DA. 1998. *Chem. Phys.* In press
73. De Silvestri S, Weiner AM, Fujimoto JG, Ippen EP. 1984. *Chem. Phys. Lett.* 112: 195–99
74. Weiner AM, De Silvestri S, Ippen EP. 1985. *J. Opt. Soc. Am. B* 2:654–61
75. de Boeij WP, Pshenichnikov MS, Wiersma DA. 1996. *Chem. Phys. Lett.* 253: 53–60
76. Fork RL, Cruz CHB, Becker PC, Shank CV. 1987. *Opt. Lett.* 12:483–85
77. Spielmann Ch, Curley PF, Brabec T, Wintner E, Kausz F. 1992. *Electron. Lett.* 28:1532–33
78. Huang CP, Asaki MT, Backus S, Murnane MM, Kapteyn HC, Nathel H. 1992. *Opt. Lett.* 17:1289–91
79. Keller U, ed. 1997. *Appl. Phys. B* 65 (Special Issue)
80. Yan YJ, Fried LE, Mukamel S. 1989. *J. Phys. Chem.* 93:8149–62
81. Allen L, Eberly JH. 1975. *Optical Resonance and Two–Level Atoms*. New York: Wiley
82. Ramaswamy M, Ulman M, Paye J, Fujimoto JG. 1993. *Opt. Lett.* 18:1822–24
83. Pshenichnikov MS, de Boeij WP, Wiersma DA. 1994. *Opt. Lett.* 19:572–74
84. de Boeij WP. 1997. *Ultrafast solvation dynamics explored by nonlinear optical spectroscopy*. PhD thesis. Univ. Groningen, The Netherlands
85. Duppen K, Wiersma DA. 1987. *Science* 237:1147–54
86. Emde MF, de Boeij WP, Pshenichnikov MS, Wiersma DA. 1997. *Opt. Lett.* 22: 1338–40
87. Bloch F. 1946. *Phys. Rev.* 70:460–74
88. Nagasawa Y, Passino SA, Joo T, Fleming GR. 1997. *J. Chem. Phys.* 106:4840–52
89. Jonas DM, Lang MJ, Nagasawa Y, Joo T, Fleming GR. 1996. *J. Phys. Chem.* 100: 12660–73
90. Cho M-H, Scherer NF, Fleming GR, Mukamel S. 1992. *J. Chem. Phys.* 96: 5618–29
91. Scherer NF, Ruggiero AJ, Du M, Fleming GR. 1990. *J. Chem. Phys.* 93:856–57
92. Scherer NF, Carlson RJ, Matro A, Du M, Ruggiero AJ, et al. 1991. *J. Chem. Phys.* 95:1487–511
93. Scherer NF, Matro A, Ziegler LD, Du M, Carlson RJ, et al. 1992. *J. Chem. Phys.* 96:4180–94
94. Kubo R. 1969. *Adv. Chem. Phys.* 15:101–27
95. Kane DJ, Trebino R. 1993. *J. Quant. Electr.* 29:571–79
96. DeLong KW, Trebino R. 1994. *J. Opt. Soc. Am. B* 11:1595–608
97. Fittinghoff DN, DeLong KW, Trebino R, Ladera CL. 1995. *J. Opt. Soc. Am. B* 12: 1955–67
98. Fittinghoff DN, Bowie JL, Sweetser JN, Jennings RT, Krümbugel MA, et al. 1996. *Opt. Lett.* 21:884–86; Erratum. 1996. *Opt. Lett*. 21:1313
99. Walecki WJ, Fittinghoff DN, Smirl AL, Trebino R, Ladera CL. 1997. *Opt. Lett.* 22:81–83
100. Papoulis A. 1962. *The Fourier Integral and Its Applications*. New York: McGraw–Hill
101. Cho M-H, Rosenthal SJ, Scherer NF, Ziegler LD, Fleming GR. 1992. *J. Chem. Phys.* 96:5033–38
102. Lotshaw WT, McMorrow D, Thantu N, Melinger JS, Kitchenham R. 1995. *J. Raman Spectrosc.* 26:571–83

103. Mokhtari A, Chebira A, Chesnoy J. 1990. *J. Opt. Soc. Am. B* 7:1551–57
104. Rosenthal SJ, Xie X-L, Du M, Fleming GR. 1991. *J. Chem. Phys.* 95:4715–18
105. Rosenthal SJ, Jimenez R, Fleming GR, Kumar PV, Maroncelli M. 1994. *J. Mol. Liq.* 60:25–56
106. Jimenez R, Fleming GR, Kumar PV, Maroncelli M. 1994. *Nature* 369:471–73
107. Horng ML, Gardecki JA, Papazyan A, Maroncelli M. 1995. *J. Phys. Chem.* 99: 17311–37
108. Gustavsson T, Baldacchino G, Mialocq J-C, Pommeret S. 1995. *Chem. Phys. Lett.* 236:587–94
109. Schoenlein RW, Mittleman DM, Shiang JJ, Alivisatos AP, Shank CV. 1993. *Phys. Rev. Lett.* 70:1014–17
110. Shank CV, Schoenlein RW, Bardeen CJ, Mittleman DM. 1994. In *Femtosecond Reaction Dynamics*, ed. DA Wiersma, pp. 125–32. Amsterdam: North Holland
111. de Boeij WP, Pshenichnikov MS, Wiersma DA. 1996. *J. Chem. Phys.* 105: 2953–60
112. Bloom AL. 1955. *Phys. Rev.* 98:1105–11
113. Schoemaker RL. 1978. In *Laser and Coherence Spectroscopy*, ed. JI Steinfeld, pp. 197–371. New York: Plenum
114. Duppen K, Wiersma DA. 1986. *J. Opt. Soc. Am. B* 3:614–21
115. Tannor DJ, Rice SA. 1988. *Adv. Chem. Phys.* 70:441–523
116. Brumer P, Shapiro M. 1989. *Acc. Chem. Res.* 22:407–13
117. Brumer P, Shapiro M. 1995. *Sci. Am.* 272:56–63
118. Hart EJ, Boag JW. 1962. *J. Am. Chem. Soc.* 84:4090–95
119. Migus A, Gauduel Y, Martin JL, Antonetti A. 1987. *Phys. Rev. Lett.* 58:1559–62
120. Long FH, Lu H, Eisenthal KB. 1990. *Phys. Rev. Lett.* 64:1469–72
121. Gauduel Y, Pommeret S, Migus A, Antonetti A. 1991. *J. Phys. Chem.* 95:533–39
122. Long FH, Lu H, Shi X, Eisenthal KB. 1991. *Chem. Phys. Lett.* 185:47–52
123. Alfano JC, Walhout PK, Kimura Y, Barbara PF. 1993. *J. Chem. Phys.* 98:5996–98
124. Kimura Y, Alfano JC, Walhout PK, Barbara PF. 1994. *J. Phys. Chem.* 98:3450–58
125. Gauduel Y. 1995. *J. Mol. Liq.* 63:1–54
126. Reuther A, Laubereau A, Nikogosyan DN. 1996. *J. Phys. Chem.* 100:16794–800
127. Pépin C, Goulet T, Houde D, Jay-Gerin J-P. 1997. *J. Phys. Chem. A* 101:4351–60
128. Kummrow A, Emde MF, Pshenichnikov MS, Wiersma DA. 1998. *J. Phys. Chem.* Submitted
129. Emde MF, Kummrow A, Pshenichnikov MS, Wiersma DA. 1998. *Phys. Rev. Lett.* Submitted
130. Schnitker J, Motakabbir K, Rossky PJ, Friesner R. 1988. *Phys. Rev. Lett.* 60:456–59
131. Rossky PJ, Schnitker J. 1988. *J. Phys. Chem.* 92:4277–85
132. Webster FJ, Schnitker J, Friedrichs MS, Friesner RA, Rossky PJ. 1991. *Phys. Rev. Lett.* 66:3172–75
133. Neria E, Nitzan A. 1993. *J. Chem. Phys.* 99:1109–23
134. Schwartz BJ, Rossky PJ. 1994. *Phys. Rev. Lett.* 72:3282–85
135. Staib A, Borgis D. 1995. *J. Chem. Phys.* 103:2642–55
136. Prezhdo OV, Rossky PJ. 1996. *J. Phys. Chem.* 100:17094–102
137. Schwartz BJ, Bittner ER, Prezhdo OV, Rossky PJ. 1996. *J. Chem. Phys.* 104: 5942–55
138. Schwartz BJ, Rossky PJ. 1996. *J. Chem. Phys.* 105:6997–7010
139. Bratos S, Leiknam J-C, Staib A, Borgis D. 1997. *Phys. Rev. E* 55:7217–27
140. Baltuška A, Wei Z, Pshenichnikov MS, Wiersma DA. 1997. *Opt. Lett.* 22:102–4
141. Baltuška A, Wei Z, Pshenichnikov MS, Wiersma DA, Scipocz R. 1997. *Appl. Phys. B* 65:175–88

Annual Review of Physical Chemistry
Volume 49, 1998

CONTENTS